

Attosecond nanoplasmonic streaking of localized fields near metal nanospheres

Frederik Süßmann and Matthias F. Kling

Max-Planck-Institut für Quantenoptik, Hans-Kopfermann-Straße 1, D-85748 Garching, Germany

Collective electron dynamics in plasmonic nanosystems can unfold on timescales in the attosecond regime and the direct measurements of plasmonic near-field oscillations is highly desirable. We report on numerical studies on the application of attosecond nanoplasmonic streaking spectroscopy to the measurement of collective electron dynamics in isolated Au nanospheres. The plasmonic field oscillations are induced by a few-cycle NIR driving field and are mapped by the energy of photoemitted electrons using a synchronized, time-delayed attosecond XUV pulse. By a detailed analysis of the amplitudes and phase shifts, we identify the different regimes of nanoplasmonic streaking and study the dependence on particle size, XUV photoelectron energy and emission position. The simulations indicate that the near-fields around the nanoparticles can be spatio-temporally reconstructed and may give detailed insight into the build-up and decay of collective electron motion.

PACS numbers: 73.20.Mf, 78.47.J-

Nanoplasmonics has rapidly evolved and numerous techniques have been developed to study the effects of plasmonic field enhancement¹, but so far the direct, time-resolved measurement of plasmonic near-fields has not been achieved. The fastest dynamics in plasmonic nanosystems can take place on timescales down to 100 attoseconds as determined from the inverse bandwidth of plasmonic resonance spectra. Attosecond metrology has provided valuable tools for measurements of ultrafast electron dynamics in atoms²⁻⁵, molecules⁶ and surfaces⁷. One of the most successful techniques is attosecond streaking spectroscopy^{8,9}, employing photoemission of electrons by an attosecond XUV pulse synchronized to a strong optical field. Recording the electron kinetic energy spectra (by e.g. time-of-flight (TOF) spectroscopy) as a function of the delay between the two pulses allows for the reconstruction of the laser fields and the electron emission dynamics. The technique is consequently a promising candidate for the real-time observation of collective electron motion in nanosystems.

One of the key aspects in traditional attosecond streaking on e.g. gas phase atomic targets is the spatial homogeneity of the driving laser field. In contrast, noble metal nanoparticles exhibit strongly enhanced, but highly localized optical fields, such that the assumption of spatial homogeneity is no longer valid. When applying attosecond streaking spectroscopy to nanoparticles, the spatial decay of the near-field into free space will govern the streaking process. Nanoplasmonic streaking was originally proposed for the instantaneous electric field probing regime¹⁰. A study on integrated streaking spectroscopy on nanostructured antennas showed, that a reconstruction of the relatively homogeneous field in the antenna gap is possible if photoemission is limited to this region¹¹. Here the electron acceleration mostly takes place in the ponderomotive regime.

We extend this previous work to spherical Au nanoparticles of different sizes and exploring the transition from the instantaneous to the ponderomotive streaking regime. By taking into account the full spatial and temporal dependence of the plasmonic near-field, we analyze

the streaking processes as a function of the nanoparticle size and laser parameters in detail. Spherical particles allow the use of Mie theory and were chosen for computational efficiency. The conclusions drawn in our study are, however, not limited to spheres, as the spatial decay of the near-field for a variety of systems shows similar, exponential behavior¹². Employing isolated nanoparticles

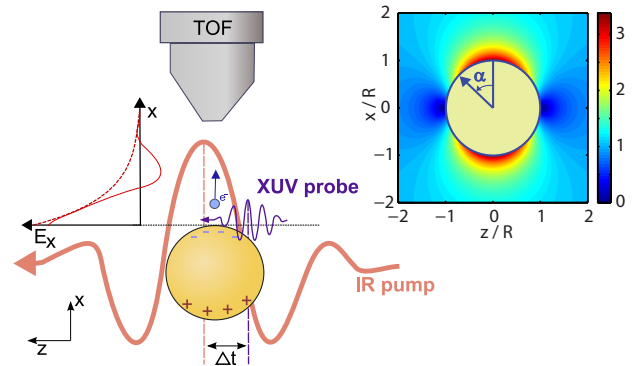


FIG. 1: (color online) Scheme for attosecond nanoplasmonic streaking of Au nanospheres employing few-cycle NIR pump pulses, attosecond XUV probe pulses and the measurement of the kinetic energies of photoemitted electrons using a time-of-flight (TOF) spectrometer. The inset shows the field enhancement as calculated by Mie theory for $y = 0$. Due to symmetry of the plasmonic field, the point of electron emission is uniquely defined by the angle α .

omits the requirement for spatially resolved experiments such as photoelectron emission microscopy, which is experimentally challenging in conjunction with attosecond light sources^{13,14}. Such isolated nanoparticles of nearly equal size and shape may be prepared by chemical synthesis in large quantities¹⁵. The nanoparticles can be supplied in sufficient density to the laser focus by employing either aerodynamic lenses^{16,17}, optical trapping¹⁸ or laser ablation¹⁹. From the experimental point of view, there are two major advantages of such an approach. First, the contrast in the spectra is expected to be higher,

as this approach does not include a substrate. Furthermore, as the particles are replaced for each laser shot, the damage threshold of the Au nanospheres²⁰ does not play a role and the non-linear plasmonic regime can be studied as well.

The scheme for attosecond nanoplasmonic streaking of fields near a metal nanosphere is depicted in figure 1. A few-cycle NIR laser pulse excites the plasmonic oscillations and a time-delayed attosecond XUV laser pulse (with a photon energy on the order of 100 eV) photoemits electrons from the nanosphere. The photoelectrons under consideration here are emitted from the Fermi edge of the conduction band. Furthermore they are assumed to not have scattered with other electrons or the lattice, which is justified if emission takes place close to the surface as the electron's mean free path is on the order of a few monolayers²¹. Accordingly the initial electron kinetic energy is given by $E_{kin} = h\nu_{xuv} - W_f$ for the XUV frequency ν_{xuv} and the work function of Au of $W_f = 5.1$ eV. While traveling to the detector, the electrons are accelerated by the local electric field near the metal nanoparticle resulting in a kinetic energy shift as a function of delay time that is measured with a TOF spectrometer. In our simulations the final drift velocity of a photoelectron (emitted at time t_e with an initial velocity \vec{v}_0) was obtained by integrating the electron's classical equation of motion

$$\vec{v}_f(t_e) = \vec{v}_0 - \int_{t_e}^{\infty} dt \frac{\vec{E}(\vec{r}, t)e}{m}, \quad (1)$$

where e is the elementary charge and m is the electron mass. The integration was performed with an explicit Runge-Kutta algorithm (4th order) using a time step of 10 as. The plasmonic response and the corresponding near-field $\vec{E}(\vec{r}, t)$ is calculated using Mie theory^{22,23}. Using this approach, the enhancement and phase shift of the electric field outside the sphere can be calculated by a normal mode expansion of the sphere's electromagnetic response. The incident, linearly polarized laser field is

$$\vec{E}(t) = E_0 \exp\left(\frac{-t^2}{\tau^2}\right) \cos(\omega t + \phi) \hat{e}_x, \quad (2)$$

with $\tau = 2.1$ fs, corresponding to a full-width at half-maximum of 5 fs, an angular frequency ω corresponding to a center wavelength of $\lambda = 720$ nm, and a carrier-envelope phase $\phi = \pi$. The Coulomb field of the charged nanoparticle after electron emission is orders of magnitude smaller than the plasmonic near-field and thus neglected.

Using the appropriate wavelength dependent dielectric function for Au fitted to experimental data, Mie theory predicts the resonance of Au spheres to be well below 600 nm for diameters up to 100 nm (see Suppl. Inf.). In turn, for these diameters the system is driven off resonance with the implication that the field enhancement as well as the phase of the enhanced near-field do not vary

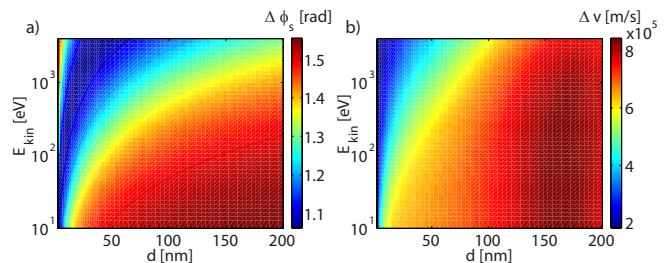


FIG. 2: (color online) a) Phase shift $\Delta\phi_s$ and b) maximum velocity shift as a function of electron energy E_{kin} and Au sphere diameter d obtained for a laser intensity of 10^{12} W/cm² and $\alpha = 0^\circ$.

significantly over the entire NIR laser spectrum. Under this condition, the calculations can be simplified and the entire laser spectrum treated with a single set of Mie coefficients for the center wavelength. The phase shift $\Delta\phi_p$ of the near-field with respect to the driving field was taken into account in the calculations, but plays only a minor role for small Au spheres. The field enhancement factor $\sigma = E_p/E_0$ for Au spheres is predicted to be between 3.4 and 4 for spheres with diameters d between 10 nm and 100 nm, respectively. Throughout this study we use parameters for which the maximum velocity shift of a photoelectron is small compared to its initial velocity, so that recollision and rescattering do not have to be taken into account. Electrons resulting from multi-photon emission and acceleration in the NIR field are neglected since for the chosen NIR intensity they are energetically well separated from the XUV emitted electrons²⁴.

First, we limit the analysis to electrons liberated from $\alpha = 0^\circ$ (see fig. 1) and traveling in x-direction corresponding to the emission along the polarization axis towards the TOF spectrometer. Significant insight can be gained from the phase shift between the streaking curve and the plasmonic near-field $\Delta\phi_s$. The phase shift serves as a measure how the streaking spectrum is generated and is in principle dependent on all experimental parameters (namely sphere diameter, electron energy, enhancement factor, duration of the near-field). Figure 2 a) shows $\Delta\phi_s$ as a function of the sphere diameter d and electron energy E_{kin} for $\tau = 2.1$ fs and an intensity of 10^{12} W/cm² of the NIR field. The size dependence of $\Delta\phi_s$ originates from the spatial extension of the near-fields into the vacuum, which is decaying with approximately $1/r^3$, with r being the radial distance from the origin. For moderate electron energies and large spheres, the phase shift is approaching $\pi/2$.

In this regime the electron velocity is small with respect to the field decay length, resulting in a ponderomotive acceleration in the plasmonic field. Decreasing the particle size at a fixed initial kinetic energy leads to a decrease of $\Delta\phi_s$. Now the regime of instantaneous near-field probing is approached, as the electrons leave the near-field faster and the acceleration is thus also confined in time. Going to even smaller particles, $\Delta\phi_s$ even-

tually increases again, because here the net acceleration by the near-field is smaller than the ponderomotive acceleration in the laser field. The minimum achievable phase shift is mainly determined by the enhancement factor σ , which defines the relative strength of the two contributions. The maximum velocity shift Δv_{max} of the streaking curve is shown in Figure 2 b). For the moderate near-field intensities used here, the velocity shift increases linearly with the electric near-field amplitude. Consequently, Δv_{max} generally follows the field enhancement factor peaking for a sphere diameter of about 170 nm. For small sizes and/or large electron energies, Δv_{max} approaches the value expected from streaking in the homogenous laser field of 2×10^{-5} m/s.

For the spherical Au particles under consideration with relatively low enhancement factors, we can conclude that a direct probing of the electric field, as was discussed in Stockman *et al.*¹⁰ is not achievable. On the other hand, the enhancement factor is large enough to give sufficient contrast in streaking spectrograms especially in the ponderomotive regime.

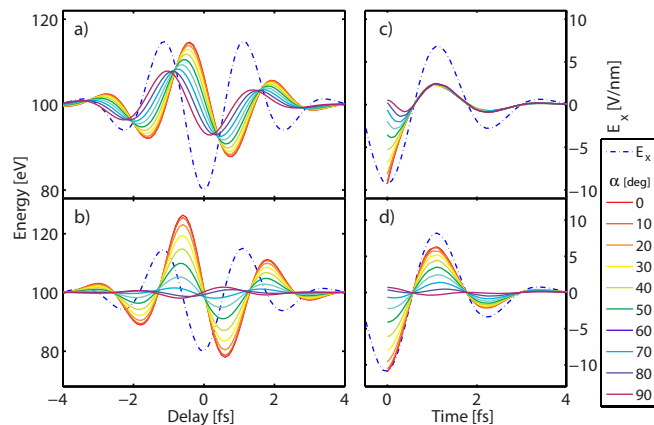


FIG. 3: (color online) Streaking traces for emission positions $\alpha = 0 - 90^\circ$ for 10 nm (a) and 100 nm spheres (b) and the respective electric fields acting on the photoelectrons (emitted at $t_e = 0$ fs) as a function of time after photoemission, (c) and (d). The blue dashed lines show the plasmonic near field.

Another important aspect arising from the spatial inhomogeneity of the plasmonic fields is the dependence of nanoplasmonic streaking on initial conditions such as emission position and launch angle. This is especially important, because XUV radiation can liberate electrons at any position on the sphere. For the following discussion the XUV photon energy is kept fixed at $h\nu_{xuv} = 105$ eV, which can routinely be produced via high-harmonic generation in Ne²⁵. Figures 3a) and b) show the influence of the emission position α on the streaking traces for 10 nm and 100 nm Au spheres, respectively. In general, for larger values of α (representing emission from a ring) the phase shift $\Delta\phi_s$ increases while the streaking amplitude decreases. This can be explained by the field distribution around the nanosphere (see figure 1). Note that the particle sizes considered here are much smaller than the

wavelength, such that the dipolar mode is dominating and all spheres show qualitatively similar field distributions.

Neglecting additional acceleration, the 100 eV photoelectrons travel about 6 nm per femtosecond. Electrons emitted on-axis ($\alpha = 0^\circ$) will show the largest energy shift and smallest phase shift $\Delta\phi_s$, as they are accelerated by the strongest near-field. Photoelectrons emitted at the sides of the sphere ($\alpha \approx 90^\circ$) initially experience weak or even opposite electric fields (with respect to $\alpha = 0^\circ$) after liberation. The electric fields acting on electrons that have left the sphere from different emission positions and travel to the detector will eventually converge. Figure 3c) and d) show the effective, time-dependent electric fields acting on electrons for 10 nm and 100 nm Au spheres, respectively. For the 10 nm sphere the fields of all emission positions have become equal after less than one half-cycle of the plasmonic field oscillation. For larger spheres this situation changes significantly. The electron travel time through the near-field approximately scales with the sphere radius. Electrons emitted from the side of e.g. a 100 nm sphere do not reach the regions of strong field enhancement before the near-field oscillations vanish (owing to the short pulse duration discussed here). Accordingly, these electrons do not show noticeable net acceleration.

The complex dependence of the electron energy shift on the initial emission conditions will determine nanoplasmonic streaking spectrograms recorded under the described geometry. A distortion of the streaking spectrograms especially for larger sizes is expected from the analysis above. To study these effects in more detail, a large number of electron trajectories with randomized initial conditions were integrated for each sphere size. The initial conditions accounted for the probabilities of the emission position, launch angle (within a 44° cone, corresponding to the acceptance angle of the TOF spectrometer), kinetic energy within the XUV spectral bandwidth (5 eV) and XUV pulse duration (200 as). Transmission of XUV through the nanosphere and emission from the back side was included in the calculations (see Suppl. Inf.). The trajectory calculations were performed for the few-cycle NIR pulses described above ($\tau = 2.1$ fs, $I = 10^{12}$ W/cm², $\phi = \pi$).

Figures 4a) and b) show streaking spectrograms composed of 1.5×10^5 electron trajectories for 10 nm and 100 nm spheres, respectively. The two streaking spectrograms are vastly different. The amplitude and phase shifts for different emission positions described above are responsible for this behavior. The typical streaking pattern is almost completely washed out in 4b) (100 nm), while it can still be observed in 4a) (10 nm). Electrons emitted from a 100 nm sphere at angles α larger than 60° are hardly accelerated. Since the statistical weight of each contribution to the spectrogram is approximately proportional to the respective area on the sphere, around 50% of the photoemitted electrons exhibit minimal energy shifts.

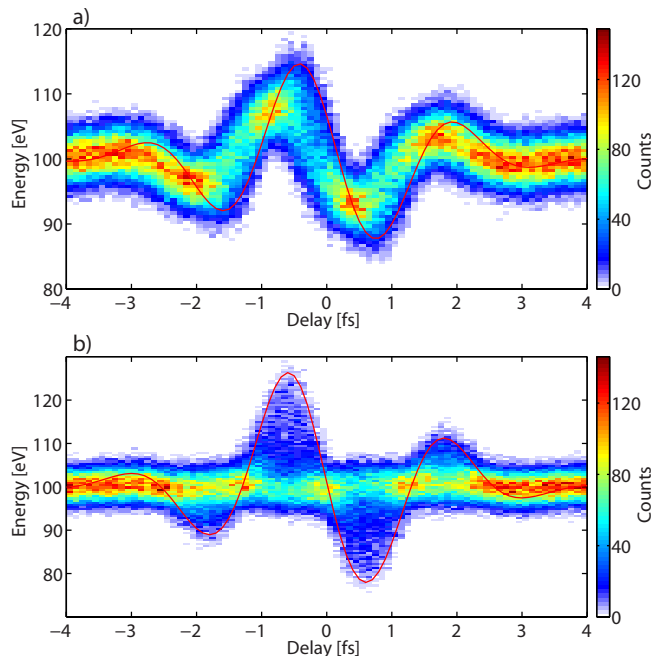


FIG. 4: (color online) Simulated streaking spectrograms for 10 nm (a) and 100 nm (b) Au spheres. The red line shows the contribution of the $\alpha = 0^\circ$ trajectories.

A streaking spectrogram recorded for a rare gas (e.g. Ne)⁹ under the same experimental conditions can serve as a reference permitting the precise reconstruction of the driving NIR field and XUV pulse parameters²⁵. Such a reconstruction is also desirable for the temporal and spatial properties of the plasmonic field. As the equation of motion of the electrons in its general form (eq. 1) is not analytically integrable, numerical simulations as presented in Fig. 4 have to be performed for the retrieval of the spatio-temporal near-fields of the nanospheres. The reconstruction could employ a feedback algorithm, which modifies the simulation parameters until best agreement with the measured spectrogram has been achieved.

Under the assumption of a constant average electron velocity and approximating the spatial near-field decay by an exponential function, an analytical integration of the equation of motion for $\alpha = 0^\circ$ trajectories is possible (see Suppl. Inf.). This allows for a computational less expensive retrieval. A major difficulty, however, lies in extracting this specific contribution from the streaking spectrogram. As can be seen in figure 4, the streaking waveform for $\alpha = 0^\circ$ (red line) can be identified more

easily for the 100 nm sphere and enables an analytic reconstruction.

In order to test the experimental implementation of attosecond nanoplasmonic streaking, we estimated the expected electron count rates using table-top attosecond XUV light sources and typical nanoparticle target densities provided by aerosol evaporation techniques¹⁶. Although we have only considered single particles in our simulations, an ensemble of nanoparticles may be utilized in an experiment for a target that provides sufficient spatial separation between individual particles. For an XUV pulse with 10^5 photons, a target density of 10^6 cm^{-3} and 100 nm Au particles we obtain a count rate of 1 s^{-1} using a 10 kHz laser system (see Suppl. Inf.). The count rate can be increased by one-three orders of magnitude by employing optical trapping methods¹⁸ or laser ablation targets¹⁹. Alternatively, an XUV light source with very high flux, such as the one expected to emerge from the European Light Infrastructure (ELI)²⁶, could be utilized.

In conclusion, we analyzed and discussed the attosecond streaking of plasmonic near-fields around isolated Au nanospheres of different diameters. In contrast to conventional attosecond streaking, the electron acceleration and deceleration has a strong spatial dependence and significant differences are identified in our simulations for 10 nm and 100 nm particles. These differences are caused by retardation effects between electron trajectories emitted from different positions on the nanosphere. The spatio-temporal information that can be retrieved from recorded streaking spectrograms could greatly deepen our understanding of how plasmons form and how they decay. In contrast to studies on nanostructured surfaces, where the field strength must remain below the damage threshold of the material, a beam of isolated nanoparticles would allow studies in the non-linear regime. Furthermore, the approach can be extended to other material groups and be used to e.g. study – in real-time - ultrafast field-induced phase transitions, such as the metallization of semiconductors and dielectrics^{27,28}.

Acknowledgments

We acknowledge discussions of this work with T. Fennel, M. Stockman, and V. Yakovlev. We are grateful for support by the DFG via SPP1391, the Emmy-Noether program and the Cluster of Excellence: Munich Center for Advanced Photonics.

¹ R. Vogelsang and A. Dimitriev, *Analyst* **135**, 1175 (2010).
² M. Drescher et al., *Nature* **419**, 803 (2002).
³ M. Uiberacker et al., *Nature* **446**, 627 (2007).
⁴ M. Schultze et al., *Science* **328**, 1658 (2010).
⁵ E. Goulielmakis et al., *Nature* **466**, 739 (2010).
⁶ G. Sansone et al., *Nature* **465**, 763 (2010).

⁷ A. Cavalieri et al., *Nature* **449**, 1029 (2007).
⁸ J. Itatani et al., *Phys. Rev. Lett.* **88**, 173903 (2002).
⁹ R. Kienberger et al., *Nature* **427**, 817 (2004).
¹⁰ M. I. Stockman et al., *Nature Phot.* **1**, 539 (2007).
¹¹ E. Skopalova et al., *New J. Phys.* **13**, 083003 (2011).
¹² P. K. Jain and M. A. El-Sayed, *Chem. Phys. Lett.* **487**,

- 153 (2010).
- ¹³ A. Mikkelsen et al., Rev. Sci. Instr. **80**, 123703 (2009).
- ¹⁴ S. Chew et al., submitted (2011).
- ¹⁵ X. Lu et al., Annu. Rev. Phys. Chem. **60**, 167 (2009).
- ¹⁶ X. Wang and P. McMurry, Aerosol Sci. Technol. **40**, 320 (2006).
- ¹⁷ S. Zherebtsov et al., Nature Phys. **7**, 656 (2011).
- ¹⁸ J. Meinen et al., Rev. Sci. Instr. **81**, 085107 (2010).
- ¹⁹ S. Noel et al., Appl. Surf. Sci. **253**, 6310 (2007).
- ²⁰ A. Plech et al., Nature Phys. **2**, 44 (2006).
- ²¹ S. Tanuma et al., Surf. Interface Anal. **17**, 911 (1991).
- ²² G. Mie, Ann. Phys. **25**, 377 (1908).
- ²³ E. C. L. Ru and P. G. Etchegoin, *Principles of Surface-Enhanced Raman Spectroscopy and Related Plasmonic Effects* (Elsevier, 2009).
- ²⁴ P. Dombi, Adv. Imaging and Electron Phys. **158**, 1 (2009).
- ²⁵ E. Goulielmakis et al., Science **320**, 1614 (2008).
- ²⁶ J.-P. Chambaret et al., Proc. SPIE **7721**, 1D (2010).
- ²⁷ M. Durach et al., Phys. Rev. Lett. **105**, 086803 (2010).
- ²⁸ M. Durach et al., Phys. Rev. Lett. p. in press (2011).